Lattice Trapping Barriers to Brittle Fracture

N. Bernstein and D.W. Hess*

Center for Computational Materials Science, Naval Research Laboratory, Washington, DC 20375, USA

(Received 22 August 2002; revised manuscript received 31 March 2003; published 8 July 2003)

We present a multiscale simulation of a crack in silicon under tensile loading that is consistent with experiment; fracture is brittle with a modest lattice-trapping energy barrier to crack propagation. Our multiscale molecular-dynamics simulation has a tight-binding description of bonding near the crack tip embedded in an empirical-potential (EP) region. Forces on atoms in the tight-binding region are computed using a Green's function method. Comparing our multiscale simulation with EP simulations shows that the EP models severely overestimate lattice trapping, explaining the failure of the Griffith criterion and the dramatic differences in crack morphology. A two-length-scale model for the lattice-trapping energy barrier correctly predicts the critical load for brittle fracture. We argue that lattice trapping plays an important role in the brittle-to-ductile transition.

DOI: 10.1103/PhysRevLett.91.025501 PACS numbers: 62.20.Mk, 34.20.Cf, 62.20.Fe, 71.15.Pd

The Griffith criterion predicts the critical load for brittle fracture by balancing the elastic energy released by crack advance against the energy of the newly formed surface [1]. The atomic nature of crystalline materials leads to an effective periodic potential for the crack tip which may include energy barriers that can arrest crack motion [2]. These lattice trapping barriers are analogous to Peierls barriers [3] to dislocation motion [2]. Lattice trapping suppresses brittle fracture up to loads larger than the Griffith critical load [4]. If lattice trapping is sufficiently large, other failure mechanisms, such as dislocation nucleation and plastic deformation, could become active before brittle fracture can occur. Studies of lattice trapping based on simplified model potentials suggest that its magnitude can vary from negligible to significant, depending on the lattice and details of the potential [5]. Since fracture experiments together with the Griffith criterion are often used to determine surface energies [6,7], significant lattice trapping would lead to a significant error in the deduced surface energy.

Experiments on silicon at low temperatures show brittle fracture at a load consistent with the Griffith criterion [8]. However, the uncertainties in the experimentally applied load and the theoretically derived surface energy make the role of lattice trapping in silicon uncertain. Quasistatic-first-principles simulations that make significant approximations of the near-crack-tip displacement field predict small but significant lattice trapping [9,10]. Simulations of fracture based on empirical potentials (EPs) are not conclusive. When used to simulate fracture, many EPs that accurately model silicon, e.g., the Stillinger-Weber (SW) [11] and the environment dependent interatomic potentials (EDIP) [12], predict ductile fracture, contradicting experiment [13,14]. A recent report of brittle fracture in an EP simulation of silicon shows fracture significantly above the Griffith criterion prediction [15], suggesting significant lattice trapping. Significant lattice trapping was also observed for a brittle but otherwise unphysical modification of the SW potential, referred to as IMSW [16,17].

Here we use a tight-binding (TB) total-energy method that describes covalent bonding more accurately and is practical for molecular dynamics (MD) simulations. We present a simulation of fracture using an atomistic multiscale method that dynamically couples EPs and TB (DCET) [18]. As shown in Fig. 1, this simulation yields dynamic brittle fracture in silicon. The onset of fracture

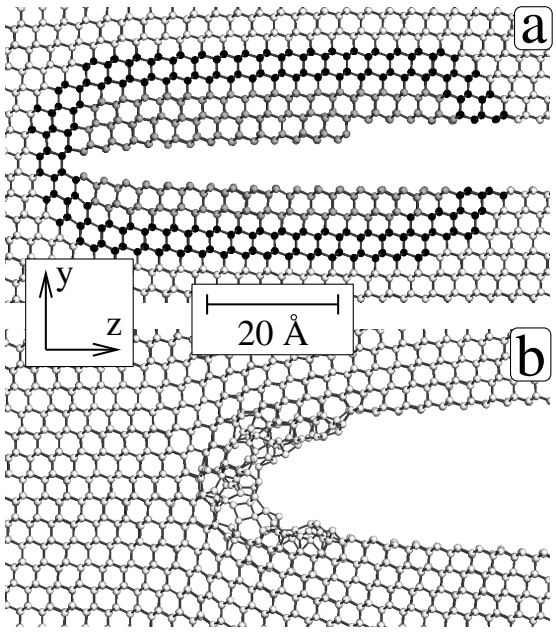

FIG. 1. Snapshots 2 ps into simulations of crack propagation using the DCET MD method (a) and the SW EP (b). White signifies atoms simulated using the EP, gray signifies atoms in the TB region, and black signifies atoms at the interface between the two regions. The temperature is 200 K and the loading G is 1.51 or 11.2 J/m^2 (applied strains of 1.7% and 5%) for the DCET MD and SW simulations, respectively.

occurs nearly at the Griffith critical load, suggesting that lattice trapping is small.

Figure 1 shows remarkable differences in fracture morphologies between otherwise accurate models of silicon. We show that lattice trapping underlies these differences. The ductile models are dominated by lattice trapping up to the critical load at which dislocations begin to form and ductile failure begins. In this way, brittle fracture is entirely suppressed by lattice trapping. We present a model that decomposes the energy barrier into bond breaking and elastic relaxation contributions. The model reproduces the large barriers we find by direct calculation for our EP simulations and predicts a tiny barrier for DCET simulations, consistent with our observation of fracture nearly at the Griffith criterion. The lattice trapping barrier is controlled by the interplay of two length scales which naturally emerge from our model, a result presaged by the analysis of Curtin [5,19]. An understanding of both scales is needed to predict the behavior of a material, whether real or simulated.

Figure 1(a) shows the partitioning of the system in our DCET simulation into a far field region and a crack-tip region, dynamically coupled through an interface region. Far from the crack tip, elastic stress fields are small and atomic motion is simulated using the EDIP EP [12,20]. Near the crack tip, stress concentration ultimately leads to bond breaking and bonding is described using a TB model [21]. Forces on atoms in this region are computed using a Green's-function-based total-energy method [22]. This method does not require artificial termination of dangling bonds and the computational effort scales linearly with the number of atoms. The interface atoms experience forces computed using the EP; constrained Green's function matrix elements involving orbitals around these atoms comprise the boundary conditions for the electronic system [22].

The simulated system consists of a $3 \times 25 \times 60$ supercell of a 12 atom $(\frac{1}{2}\bar{\frac{1}{2}}0) \times (11\bar{1}) \times (\bar{\frac{1}{2}}\bar{\frac{1}{2}}\bar{1})$ unit cell (these directions define x, y, and z, respectively). Periodic boundary conditions are used along x and z, while the boundaries along y, the tensile loading direction, are fixed. A seed crack, with $(11\bar{1})$ faces and a $\langle 1\bar{1}0\rangle$ crack front, extending through the entire system along x and 198.6 Å (half the system size) along z is introduced. The isotropic elastic displacement field for a thin crack in an infinite plate [23] provides the mechanical loading of the sample. The TB region, which extends ~17 Å along y and ~55 Å along z, includes one of the tips of the seed crack, is fixed during the simulation, and is surrounded by a 6.5 Å transition layer. The MD time evolution is computed using the velocity Verlet algorithm [24] with a 1 fs time step.

A visualization of a DCET MD simulation [Fig. 1(a)] shows brittle fracture. As the crack tip advances, it remains atomically sharp and newly generated surface is atomically smooth. There is no sign of disorder, dislocations, or a plastic zone. The analogous simulation using only SW [Fig. 1(b)] shows a blunt crack tip surrounded by a disordered region, consistent with ductile fracture.

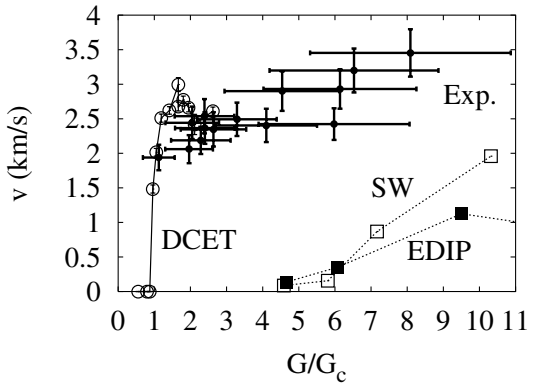

FIG. 2. Crack speed as a function of loading for DCET MD, SW, EDIP, and the experiment of Ref. [8] (solid circles). Loading is measured in terms of the energy release rate scaled to the G_c for each model or experiment (see text). The onset of IMSW (not shown for clarity) is at ~2.1.

Crack speeds as a function of applied load from our simulations appear in Fig. 2 together with the result of the experiments of Ref. [8]. The load is measured in terms of the energy release rate G, which is the elastic energy released per unit length advance of the crack tip. To properly compare the onset of fracture in different models, we normalize the load by the critical energy release rate at the Griffith criterion G_c tabulated in Table I. The experiment is consistent with an onset for fracture just above G_c, as computed using the density functional theory surface energy [9]. In agreement with experiment, the DCET MD simulation shows a propagating crack when the energy release rate reaches G_c, as computed using the TB surface energy and the EDIP unrelaxed elastic constants [25]. The scatter in the measured crack speeds makes the variations at loads above the critical load statistically insignificant. In the SW and EDIP simulations, the critical energy release rate is between 6 and 7 times the appropriate G_c for each.

While the fracture morphology differences between the DCET MD and the ductile EP simulations are striking, the crucial discrepancy exists at loads below the critical load for crack propagation but above G_c. Using quasistatic energy minimization calculations, we have measured the critical loading G_c^{QS} at which bond

TABLE I. Griffith critical load, measured lattice trapping, and lattice-trapping-model parameters for Si (111) fracture.

	TB	SW	IMSW	EDIP
G_c (J/m^2)	2.0	2.8	2.8	2.2
R	1.09–1.16	1.44–1.56	1.39–1.52	1.65–1.73
s_{bb} (Å)	2.70	1.40	1.40	0.77
s_{eq} (Å)	1.38	2.31	2.00	2.34

rearrangement occurs at the crack tip. The lattice trapping measure $R \equiv \sqrt{G_c^{\mathrm{QS}}/G_c}$ is listed in Table I. The disagreement between the EPs and DCET MD appears in the form of higher lattice trapping long before dislocation nucleation begins to blunt the crack tip. The IMSW EP fractures in a brittle manner, but like SW, lattice trapping is large.

To quantify the lattice trapping barrier, we decompose the energy changes during the propagation of a crack by one lattice spacing into a bond breaking part and an elastic relaxation part. In Fig. 3 we illustrate this decomposition for SW at G_c. The energy barrier for the crack propagation process $E_{\mathrm{tot}}(s)$ is computed directly by a series of constrained minimizations at increasing crack-tip atom separations s [see Fig. 3(a)]. The bond-breaking energy $\gamma_s(s)$ is computed by separating two rigid slabs to form a new surface. The interatomic distance needed to break a bond s_{bb} (see Fig. 3) sets the length scale over which $\gamma_s(s)$ varies. The elastic energy gain, $E_{\mathrm{el}}(s) \equiv E_{\mathrm{tot}}(s) - \gamma_s(s)$, also depends on the separation of the crack-tip atoms, since that separation controls how much the rest of the loaded sample can relax. The length scale over which the elastic energy is gained is the distance between two atoms immediately behind the crack tip s_{eq} (see Fig. 3). These two length scales are listed in Table I. The balance between $E_{\mathrm{el}}(s)$ and $\gamma_s(s)$ determines the size of any energy barrier to crack propagation. The energy-barrier calculation and decomposition procedure has been repeated at several loadings using SW, IMSW, and EDIP. We find that the scaled elastic energy $E_{\mathrm{el}}(s/s_{\mathrm{eq}})/G$ is model independent. It is impractical to directly compute the barrier using DCET. To estimate the barrier using the model, we compute G using the EDIP elastic constants and obtain s_{eq} from a quasistatic DCET relaxation below G_c. By summing the scaled elastic and surface energies, we can estimate the DCET crack propagation barrier.

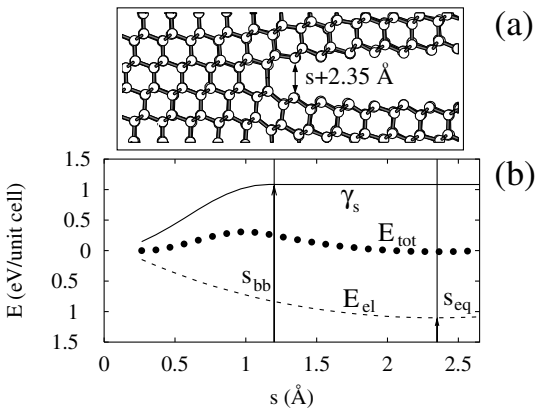

FIG. 3. (a) Visualization of an atomic configuration indicating crack-tip atom separation s. (b) Example calculation of energy decomposition for SW during the propagation of a crack at $G_c = 2.27\ \mathrm{J/m^2}$ as a function of the distance between the atoms initially at the crack tip. $E_{\mathrm{tot}}(s)$ and $\gamma_s(s)$ are computed directly (see text), and their difference is defined as $E_{\mathrm{el}}(s)$.

Figure 4(a) shows that the barriers estimated from our model and those directly computed for SW and IMSW are in good agreement. For SW, the barrier is so large that even at the critical loading for dislocation formation, the barrier to brittle fracture remains substantial. This is why brittle fracture is entirely suppressed in SW. EDIP exhibits similar behavior. In contrast, at the loading where brittle fracture is initiated for IMSW, the estimated barrier essentially vanishes, signifying the onset of brittle fracture for this EP. The modification of SW that leads to IMSW increases bond bending energies, leading to higher dislocation nucleation energies but leaving the lattice trapping barrier essentially unchanged.

The DCET barrier appears in Fig. 4(b). At G_c the crack tip is lattice trapped, with the crack-tip bond slightly stretched. At the critical loading for the initiation of brittle fracture, the estimated DCET barrier goes to zero. This indicates that the model also correctly predicts the onset of brittle fracture in the DCET simulation.

The bond-breaking energy can be modeled by the energy required to separate two rigid slabs forming ideal surfaces, i.e., bulk terminated and unrelaxed. This indicates that the bond-breaking process is not significantly affected by the relaxation of the newly formed surface, nor is it affected by the strain gradient or by the asymmetry of broken bonds on one side of the crack tip and intact bonds on the other. The model independence of the scaled elastic energy indicates that the only relevant deviation from linear elasticity is in the detailed shape of the crack immediately behind the tip.

In contrast to physical pictures where the range of the interaction is the only length scale [13,26] but similar to Ref. [5], two length scales naturally emerge from our

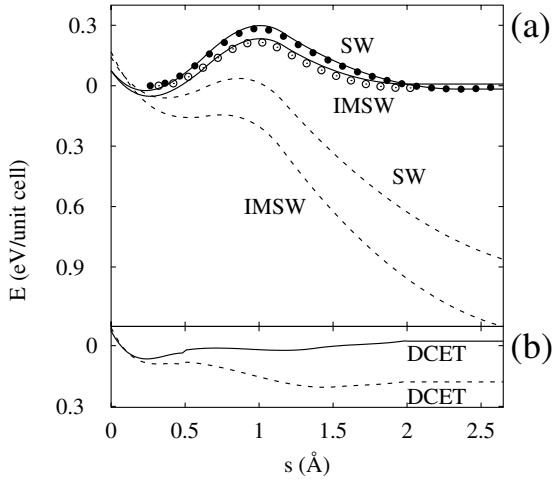

FIG. 4. (a) Energy of the crack-propagation process as computed directly at G_c (symbols), estimated using our model at G_c (solid lines), and estimated at G_c^{QS} (dashed lines). (b) Estimated energy of the crack-propagation process computed using the model for DCET MD at G_c (solid line) and at G_c^{QS} (dashed line).

model, one for bond breaking and the other for elastic relaxation. It is their relative size that is important. If the bond-breaking length scale is larger than the elastic relaxation length scale, the breaking of a single bond happens gradually as the crack advances by several lattice periods, and lattice trapping is small. In the opposite limit, all of the bond-breaking energy cost occurs before elastic relaxation lowers the total energy, and lattice trapping is large. Insofar as s_{bb} and s_{eq} approximate these length scales, Table I shows that both length scales "conspire" to reduce lattice trapping in TB as compared with the EPs: The bond-breaking distance is larger by a factor of 2–3, and the crack-tip opening at a given strain is smaller by 25%–40%.

At ~575 °C silicon exhibits an abrupt transformation from brittle fracture to ductile flow [27]. Rice's criterion and the temperature dependence of dislocation mobility have been invoked as a possible explanation of this brittle-to-ductile transition [28]. In the spirit of our model, it seems plausible that silicon's incipient ductility is controlled by the interplay between the free energy barrier to brittle fracture and the barriers to dislocation nucleation and migration. At low temperature, the barrier to brittle fracture is lower than the relevant dislocation energy scales. In silicon, the difference between these energy scales is small, temperature dependent, and sensitive to the stress field leading to the sharp brittle to ductile transition observed in experiments.

We have compared the onset of fracture in multiscale simulations and empirical potential simulations to address the significance of lattice trapping in silicon. Our multiscale model shows that lattice trapping is small but important. Popular empirical potentials show erroneously large lattice trapping, often leading to a ductile crack morphology. The lattice-trapping barrier to brittle fracture is controlled by two length scales. We suggest that lattice trapping may play a crucial role in the brittle-to-ductile transition. We are working to understand the two length scales at a first-principles level, and to determine whether the brittle-to-ductile transition is contained in the models that underlie our multiscale simulation.

The DOD HPC Challenge program and the DOD HPCMPO provided grants of computer time at the ASC MSRC and MHPCC DSRC. We acknowledge the support of the Office of Naval Research. N. B. also acknowledges the DOD HPCMPO CHSSI program, and D. W. H. the National Science Foundation.

*Current address: Division of Materials Research, National Science Foundation, Arlington, VA 22230, USA.

[1] A. A. Griffith, Philos. Trans. R. Soc. London A **221**, 163 (1921).
[2] B. Lawn, *Fracture of Brittle Solids* (Cambridge University Press, Cambridge, 1993), p. 148.
[3] J. P. Hirth and J. Lothe, *Theory of Dislocations* (McGraw-Hill, New York, 1968).
[4] R. Thomson, C. Hsieh, and V. Rana, J. Appl. Phys. **42**, 3154 (1971).
[5] W. A. Curtin, J. Mater. Res. **5**, 1549 (1990).
[6] J. J. Gilman, J. Appl. Phys. **31**, 2208 (1960).
[7] K. Kendall, N. M. Alford, and J. D. Birchall, Nature (London) **325**, 794 (1987).
[8] J. A. Hauch, D. Holland, M. P. Marder, and H. L. Swinney, Phys. Rev. Lett. **82**, 3823 (1999).
[9] J. C. H. Spence, Y. M. Huang, and O. Sankey, Acta Metall. Mater. **41**, 2815 (1993).
[10] R. Perez and P. Gumbsch, Phys. Rev. Lett. **84**, 5347 (2000).
[11] F. H. Stillinger and T. A. Weber, Phys. Rev. B **31**, 5262 (1985).
[12] J. F. Justo, M. Z. Bazant, E. Kaxiras, V. V. Bulatov, and S. Yip, Phys. Rev. B **58**, 2539 (1998).
[13] D. Holland and M. Marder, Adv. Mater. **11**, 793 (1999).
[14] F. F. Abraham, N. Bernstein, J. Q. Broughton, and D. Hess, MRS Bull. **25**, 27 (2000).
[15] J. G. Swadener, M. I. Baskes, and M. Nastasi, Phys. Rev. Lett. **89**, 085503 (2002).
[16] D. Holland and M. Marder, Phys. Rev. Lett. **80**, 746 (1998).
[17] D. Holland and M. Marder, Phys. Rev. Lett. **81**, 4029 (1998).
[18] N. Bernstein and D. W. Hess, in *Multiscale Modeling of Materials—2000*, edited by L. P. Kubin, R. L. Selinger, J. L. Bassani, and K. Cho, MRS Symposia Proceedings Vol. 653 (Materials Research Society, Warrendale, 2001), p. Z2.7.1.
[19] Unlike Ref. [5] we find that lattice trapping can be significant for realistic interatomic interactions, and that the two length scales are force model dependent.
[20] To improve the matching of mechanical properties, the parameter that sets the length scale for EDIP (parameter c of Ref. [12]) was rescaled to reduce the equilibrium lattice constant to the TB model value of 5.406 Å.
[21] N. Bernstein and E. Kaxiras, Phys. Rev. B **56**, 10 488 (1997).
[22] N. Bernstein, Europhys. Lett. **55**, 52 (2001).
[23] K. B. Broberg, *Cracks and Fracture* (Academic Press, San Diego, 1999), p. 132.
[24] M. Tuckerman, B. J. Berne, and G. J. Martyna, J. Chem. Phys. **97**, 1990 (1992).
[25] The calculation of G as a function of nominal applied strain is affected by several factors, including variations in the actual strain due to the approximate nature of the initial atomic positions, and the choice of unrelaxed vs relaxed and EDIP vs TB elastic constants. However, these should not qualitatively change the result.
[26] F. F. Abraham and J. Q. Broughton, Comput. Mater. Sci. **10**, 1 (1998).
[27] J. Samuels and S. G. Roberts, Proc. R. Soc. London A **421**, 1 (1989).
[28] J. R. Rice and G. E. Beltz, J. Mech. Phys. Solids **42**, 333 (1994).